Environ Monit Assess (2026) 198:1277
https://doi.org/10.1007/s10661-026-16115-1

RESEARCH

Assessing fire severity patterns and carbon sink capacity changes following the 2021 Manavgat wildfire using remote sensing and Google Earth Engine

Halil Duymuş

Received: 3 May 2026 / Accepted: 22 October 2026
© The Author(s), under exclusive licence to Springer Nature Switzerland AG 2026

Abstract Wildfires can impair vegetation productivity well beyond the fire year, yet the persistence and monetary implications of these deficits remain poorly characterised in Mediterranean landscapes. This study integrates Sentinel-2 burn-severity mapping, MODIS annual net primary production (NPP), an adjacent unburned-forest comparison, and scenario-based valuation to assess the 2021 Manavgat wildfire in Türkiye. A MODIS burned-area event envelope covered 424 km^2, including 270 km^2 of pre-fire forest; valid paired Sentinel-2 observations supported severity classification across 246.26 km^2. Burn-severity thresholds derived from the study-area differenced Normalized Burn Ratio (dNBR) distribution were 0.316 and 0.613. Relative to the 2016–2020 mean (0.830 kg C m^{-2} yr^{-1}), burned-forest NPP declined to 0.621 in 2021 and 0.440 in 2022, then increased to 0.705 in 2023 and 0.710 in 2024. A difference-in-differences comparison with nearby unburned forest indicated persistent productivity deficits beyond shared temporal variability. The estimated cumulative productivity-based carbon sink deficit for 2021–2024 was 227,150 t C (832,885 t CO_2e). Valuation was approximately USD 158.2 million under the central social cost of carbon scenario and EUR 60.5 million using annual EU Allowance prices. These findings demonstrate the value of integrating severity, productivity trajectories, and economic scenarios for post-fire monitoring and restoration prioritisation.

Keywords Post-fire recovery · DNBR · Ecosystem service valuation · Sentinel-2 · Mediterranean forests

Introduction

The Mediterranean Basin is among the regions most vulnerable to climate change, where rising temperatures, declining summer precipitation, prolonged drought, and increasingly frequent heat extremes are intensifying pressure on terrestrial ecosystems and wildfire regimes. The Intergovernmental Panel on Climate Change (IPCC) and the First Mediterranean Assessment Report both identify the Mediterranean as a climate-change hotspot in which warming and increasing water stress are expected to adversely affect forest health, ecosystem productivity, and fire risk (Ali et al., 2022; MedECC, 2020). These changes are particularly important for Mediterranean forest ecosystems, where climatic constraints interact with fuel conditions, topography, and human activities to influence both wildfire occurrence and severity (Jones et al., 2022; Pausas & Keeley, 2021).

These regional trends were clearly manifested during the extreme 2021 wildfire season in southwestern Türkiye. Large fires affected extensive areas

H. Duymuş (✉)
Department of Landscape Architecture, Faculty of Architecture, Çukurova University, Sarıçam, Adana 01330, Turkey
e-mail: hduymus@cu.edu.tr

Published online: 03 November 2026

of Antalya and Muğla provinces, with the Manavgat wildfire representing one of the most destructive events of the season. Multi-temporal remote-sensing assessments indicate that the Manavgat fire affected approximately 47,824 ha, with a substantial proportion of the burned area developing during the first days of the event. The extreme meteorological conditions accompanying the fire, including the 44.8 °C temperature recorded in Antalya on 3 August 2021, further illustrate the climatic context under which the event occurred (Çamalan et al., 2023; Kavzoğlu et al., 2021).

Although burned-area extent is an important indicator of wildfire magnitude, ecological effects are rarely spatially uniform. Burn severity reflects the degree of change caused by fire to vegetation, surface organic matter, and related ecosystem properties and therefore provides information that cannot be obtained from a simple burned/unburned classification. Remote sensing has become a fundamental tool for assessing such spatial heterogeneity. In particular, the Normalized Burn Ratio (NBR) and differenced Normalized Burn Ratio (dNBR) have been widely used to quantify spectral changes associated with fire impacts, while Sentinel-2 imagery enables these patterns to be mapped at comparatively fine spatial resolution (Howe et al., 2022; Key & Benson, 2006; Roy et al., 2006).

Previous studies of the 2021 Türkiye wildfires have demonstrated the value of satellite observations for characterising fire progression and ecological impacts. Kavzoğlu et al. (2021) analysed the temporal development of the Manavgat wildfire using multi-temporal remote-sensing data. Yılmaz et al. (2023) combined dNBR- and dNDVI-based severity assessment with Sentinel-5P observations to investigate burn severity and atmospheric carbon monoxide enhancements, while Aydın-Kandemir and Demir (2023) examined biodiversity and habitat impacts. More recently, Altay and Türker (2026) confirmed the applicability of Sentinel-2-based NBR and NDVI indicators for burned-area and severity assessment in the Manavgat landscape. A complementary remote-sensing investigation of the same wildfire documented widespread increases in land surface temperature and differences in thermal response between coastal and inland areas (Özenen-Kavlak et al., 2026).

A notable gap remains in the existing literature on the 2021 Manavgat wildfire: previous studies have primarily focused on burned-area delineation, spectral fire-severity assessment, atmospheric effects, or biodiversity impacts, whereas the multi-year evolution of productivity-based carbon sink losses, their persistence after accounting for regional climatic variability, and their economic implications have not been examined together within a unified analytical framework. This distinction is important because wildfire effects extend beyond immediate biomass combustion. Changes in vegetation productivity following fire can persist for several years and may vary substantially according to fire severity, ecosystem characteristics, post-fire climate, and management conditions (Ermitão et al., 2024; Fernández-Manso et al., 2016; Peña-Molina et al., 2024; Serrano-Ortiz et al., 2011).

Net primary production (NPP) provides a useful satellite-derived indicator for assessing changes in vegetation productivity and biomass accumulation over time. Although NPP does not represent a complete ecosystem carbon budget, multi-year NPP observations can provide a consistent proxy for evaluating changes in productivity-based carbon sink function. Distinguishing fire-related productivity losses from concurrent regional climatic variability is particularly important in drought-prone Mediterranean environments. Furthermore, translating carbon sink deficits into economic terms can extend biophysical assessment toward decision support. Social Cost of Carbon estimates and carbon-market prices provide two conceptually different approaches for illustrating the potential societal and market-related significance of lost carbon sink services (Bayer & Aklin, 2020; Rennert et al., 2022).

Against this background, this study integrates Sentinel-2-based fire-severity mapping, MODIS-derived annual NPP observations, a control-area difference-in-differences framework, and scenario-based economic valuation to assess the consequences of the 2021 Manavgat wildfire. Rather than estimating a complete ecosystem carbon budget, the study specifically evaluates productivity-based carbon sink capacity and its post-fire trajectory. The study addresses four research questions:

(i) How was burn severity spatially distributed across the forest areas affected by the 2021 Manavgat wildfire?
(ii) How did NPP-based carbon sink function change from the pre-fire reference period

through 2021–2024, and what recovery trajectory emerged during the first three post-fire years?

(iii) To what extent did productivity deficits persist after accounting for regional climatic variability using an unburned-forest control area and a difference-in-differences framework?

(iv) What is the magnitude of the economic value associated with the estimated carbon sink losses under Social Cost of Carbon and EU Allowance price scenarios?

By addressing these questions within a common spatial and temporal framework, the study aims to advance understanding of the ecological persistence and economic significance of post-fire carbon sink loss and to provide information relevant to severity-based restoration prioritisation and long-term carbon management in Mediterranean forest landscapes.

Materials and methods

Study area and research design

This study evaluates the impact of the wildfire that ignited on 28 July 2021 in the Manavgat district of Antalya province on productivity-based carbon-sink function. The spatial analysis domain was defined by intersecting the Manavgat administrative boundary with 2021 burn detections from the MODIS MCD64A1 product, resulting in an event-level burn envelope of 424 km^2. Because MCD64A1 has a spatial resolution of 500 m, this geometry was not interpreted as a pixel-accurate fire perimeter; rather, it was used to define the broad spatial extent of the wildfire event and to constrain subsequent analyses. Overlay with the pre-fire CORINE forest mask identified 270 km^2 of forest within this MODIS-derived event envelope. Fine-scale spatial variation in fire effects was subsequently characterised independently using Sentinel-2-derived dNBR at a 20 m analysis scale. The temporal design comprises a pre-fire reference period (2016–2020), the fire year (2021), and a post-fire recovery period (2022–2024).

The core analytical logic of the study is to map burn severity using high-spatial-resolution Sentinel-2 imagery and then to quantify changes in carbon sink capacity by linking fire impact to MODIS annual NPP data. A five-year reference mean (2016–2020) was used to reduce the influence of inter-annual meteorological variability. All analyses were carried out on the Google Earth Engine (GEE) cloud-computing platform (Gorelick et al., 2017).

Datasets

The MODIS MCD64A1 Version 6.1 Burned Area product was used to identify the event-level burn envelope and approximate burn timing. The monthly product is provided at 500 m spatial resolution and records the approximate day of burning as a Julian day in the BurnDate band; burned-area detection is based on MODIS surface-reflectance observations together with active-fire information (Giglio et al., 2018). Only valid land pixels satisfying the adopted quality criteria were retained. Given its 500 m spatial resolution, MCD64A1 was not treated as a fine-scale fire-boundary product in this study. Instead, it provided the broad spatial envelope within which Sentinel-2 imagery was subsequently used to characterise burn-severity patterns at a 20 m analysis scale.

The Sentinel-2 Surface Reflectance Harmonized collection (COPERNICUS/S2_SR_HARMONIZED) was used to characterise burn severity. This collection harmonises the radiometric offset introduced by the change in processing baseline (Baseline 04.00) that occurred at the start of 2022, thereby placing pre- and post-change scenes on a consistent reflectance scale. The near-infrared B8 band (10 m) and the shortwave-infrared B12 band (20 m) were used for NBR computation; the analysis was executed within a 20 m resolution workflow.

The MODIS/061/MOD17A3HGF Version 6.1 annual NPP product was used as the productivity-based proxy for carbon sink capacity. The product provides annual NPP at a spatial resolution of 500 m, with the NPP band expressed using a scale factor of 0.0001. MOD17 is based on a radiation-use-efficiency modelling framework in which absorbed photosynthetically active radiation is combined with MODIS-derived fraction of absorbed photosynthetically active radiation (FPAR) and leaf area index (LAI), biome-specific physiological parameters, and meteorological constraints, including temperature and vapour-pressure deficit, to estimate gross primary productivity (GPP). Autotrophic respiration is subsequently accounted for

to derive NPP. In the gap-filled MOD17 product, poor-quality FPAR/LAI observations are temporally filled to improve the continuity of the productivity estimates. Annual NPP is generated from the accumulation of within-year productivity terms derived from the 8-day MOD17 sequence (Running et al., 2004; Zhao et al., 2005).

The CORINE Land Cover 2018 (CLC 2018) raster product was used to construct the pre-fire forest mask. This pan-European land-cover inventory contains 44 thematic classes at 100 m resolution (Feranec et al., 2007); classes 311 (Broad-leaved forest), 312 (Coniferous forest), and 313 (Mixed forest) were used to represent pre-fire forested areas.

Pre-processing

Sentinel-2 images were filtered by study-area boundary and defined date windows. The pre-fire composite spans 1 June–27 July 2021, and the post-fire composite spans 1 September–31 October 2021; these windows represent, respectively, the period immediately preceding ignition and the period in which active burning and dense smoke had subsided. Pixel-level cloud masking was applied by combining a cloud probability threshold of 40% derived from the COPERNICUS/S2_CLOUD_PROBABILITY collection with Scene Classification Layer (SCL)-based masking to suppress cloud, cloud shadow, thin cirrus, and snow/haze effects (Zhu et al., 2015). Composites were generated using the median aggregation method.

Sentinel-2 bands B8 and B12 were used to calculate NBR. B8 has a native spatial resolution of 10 m, whereas B12 is provided at 20 m. No explicit bilinear or bicubic resampling operation was applied to B8 prior to NBR calculation. Instead, NBR and dNBR outputs were evaluated within a 20 m analysis workflow, with the analysis scale explicitly specified as 20 m for the relevant reductions and exports. Under Google Earth Engine's projection model, any implicit reprojection required when combining the differently resolved bands therefore used the platform's default nearest-neighbour resampling. The derived dNBR layer was subsequently assigned a 20 m default analysis projection before its aggregation to the 500 m MOD17 grid.

Event envelope and fire severity mapping

For July–August 2021, MCD64A1 pixels satisfying BurnDate > 0 and the adopted QA criteria were used to define the event-level burn envelope. Within this envelope, fire severity was assessed from the NBR and dNBR calculated from the pre- and post-fire Sentinel-2 composites. Thus, MCD64A1 was used to constrain the event domain and approximate burn timing, whereas the Sentinel-2-derived dNBR surface provided the fine-scale basis for characterising spatial variability in fire effects. Only pixels retaining valid paired pre- and post-fire Sentinel-2 observations after image-quality masking and mask harmonisation were eligible for dNBR-based severity classification. Burned-forest-mask pixels for which a valid paired dNBR value could not be obtained were excluded from the low-, moderate-, and high-severity classes and were recorded separately as a no-data/processing subset. Consequently, the residual area does not represent an additional burn-severity category. NBR is defined as the normalised difference between the near-infrared and shortwave-infrared bands:

$$\mathrm{NBR} = (\mathrm{NIR} - \mathrm{SWIR})/(\mathrm{NIR} + \mathrm{SWIR}) \quad (1)$$

In this study, dNBR was computed as:

$$dNBR = NBR_pre - NBR_post \quad (2)$$

dNBR was treated as the primary analysis variable in continuous form (Miller & Thode, 2007). Low-, moderate-, and high-severity classes were additionally generated for spatial summarisation and mapping. The classification thresholds were derived from the empirical dNBR distribution of valid burned-forest pixels within the study-area classification domain. The 33rd and 67th percentiles were calculated once, yielding p33 = 0.316 and p67 = 0.613. These threshold values were subsequently applied consistently to all valid burned-forest pixels included in the severity classification: values below p33 were assigned to the low-severity class, values between p33 and p67 to the moderate-severity class, and values above p67 to the high-severity class. Accordingly, the thresholds were fixed during classification but were study-area-specific because they were empirically derived from the Manavgat dNBR distribution rather than adopted from an externally prescribed universal threshold scheme.

Carbon sink capacity change

In this study, carbon sink capacity is treated as a productivity-based proxy via annual NPP rather than as net ecosystem carbon balance. After applying the 0.0001 scale factor to the MOD17A3HGF product, the 5-year reference mean was computed as:

$$NPP_ref = (1/5) \times \Sigma NPP_y(y = 2016, 2017, 2018, 2019, 2020) \quad (3)$$

The anomaly for each post-fire year is defined as:

$$\Delta NPPi, t = NPPi, t - NPPi, ref \quad (4)$$

where $\Delta NPP_{i,t}$ represents the NPP anomaly for analysis pixel i in year t. Negative values indicate lower productivity relative to the pre-fire reference period. Annual carbon loss was calculated only from negative NPP anomalies within the burned-forest analysis mask as:

$$C_{loss,t} = \frac{\sum_i \left[\max\left(0, -\Delta NPP_{i,t}\right) \times A_i\right]}{1000} \quad (5)$$

where A_i is the area of analysis pixel i in square metres (m^2). Because $\Delta NPP_{i,t}$ is expressed in kg C m^{-2} yr^{-1}, multiplication by pixel area yields kg C yr^{-1}; division by 1000 converts the result to tonnes of carbon (t C). Only negative anomalies were included in the loss calculation, whereas pixels with NPP equal to or greater than their reference value contributed zero to $C_{loss,t}$.

The resulting carbon loss was subsequently converted to CO_2 equivalent by applying the IPCC stoichiometric conversion coefficient of 44/12 (Harris et al., 2021; Pellegrini et al., 2018):

$$C_{loss}, CO2e(t) = C_{loss}(tC) \times (44/12) \quad (6)$$

The recovery level was assessed as the ratio of mean annual NPP in burned cells to the reference mean:

$$Recovery_t(\%) = (NPP_burn, t/NPP_burn, ref) \times 100 \quad (7)$$

This indicator was calculated separately for 2022, 2023, and 2024, yielding the recovery trajectory that traces how closely the carbon sink function approaches its pre-fire level.

Control area design and scale harmonisation

Control cells were selected outside the MCD64A1-derived event envelope but within the surrounding forest landscape to provide a reference for regional temporal variability unrelated to direct burning. The selection criteria were: (i) classification as forest in CLC 2018; (ii) absence of a 2021 burn detection in MCD64A1; and (iii) location within a 5 km buffer ring surrounding the event envelope. The use of nearby unburned areas as temporal references is consistent with previous satellite-based wildfire studies. Wang and Zhang (2017), for example, used an unburned buffer zone outside the Hayman Fire scar as a reference for comparing MODIS-derived vegetation phenology before and after wildfire, while Wang and Zhang (2020) extended burned-versus-unburned reference-area comparisons across multiple western U.S. forest fires using MODIS time series. These studies provide methodological precedent for distinguishing disturbance-related vegetation changes from broader temporal variability using spatially adjacent reference areas (Wang & Zhang, 2017, 2020).

Because the Sentinel-2-derived dNBR layer has a 20 m analysis resolution whereas the MOD17 NPP product is provided at 500 m, spatial harmonisation was required before linking fire severity and productivity information. The dNBR, burned-area fraction, and forest-fraction layers were aggregated to the MOD17 analysis grid using Google Earth Engine's *setDefaultProjection()* and *reduceResolution()* functions. The final analysis units were MOD17 cells containing pre-fire forest and a burned-area fraction of at least 60%, a criterion used to reduce mixed-pixel contributions. The spatial scale and coordinate-reference parameters were explicitly specified in the relevant regional-reduction operations.

The selected reference area was subsequently incorporated into a difference-in-differences (DID) framework to estimate the productivity deficit associated with the wildfire after accounting for temporal changes also observed in nearby unburned forest. The conceptual logic is related to the burned-versus-unburned temporal comparisons used in previous satellite-based wildfire studies (Wang & Zhang, 2017, 2020), although the present study formalises this comparison using a DID estimator applied to annual NPP. The net effect for year was calculated as:

$$NetEffect_t = (NPP_t, burn - NPP_ref, burn) - (NPP_t, ctrl - NPP_ref, ctrl) \quad (8)$$

where NPP_burn,t and NPP_ctrl,t represent mean NPP in the burned and control areas, respectively, in year, and NPP_burn,ref and NPP_ctrl,ref represent their corresponding 2016–2020 pre-fire reference means. Negative values indicate an additional productivity deficit in the burned area beyond the contemporaneous change observed in the unburned reference area. The DID framework was used as a quasi-experimental robustness assessment rather than as evidence of experimental causality, because its interpretation depends on the comparability of treated and control areas and, particularly, on the parallel-trends assumption (Callaway & Sant'Anna, 2021).

Economic valuation

Economic valuation was performed under two scenarios. In the first scenario, Social Cost of Carbon ($SCCO_2$) values published by the U.S. Environmental Protection Agency (EPA, 2023) were used: low (120 USD tCO_2^{-1}), central (190 USD tCO_2^{-1}), and high (340 USD tCO_2^{-1}) cases, all reported in 2020 U.S. dollars (Rennert et al., 2022). In the second scenario, market-based valuation was adopted using annual average EU Allowance (EUA) prices from the EEX exchange (Bayer & Aklin, 2020). EUA prices applied were: 2021: 53.4 EUR tCO_2^{-1}; 2022: 81.0 EUR tCO_2^{-1}; 2023: 85.5 EUR tCO_2^{-1}; 2024: 65.0 EUR tCO_2^{-1}. Annual monetary loss was calculated as:

$$Value_SCC, t = C_loss, CO2e, t \times SCC \quad (9)$$

$$Value_EUA, t = C_loss, CO2e, t \times P_EUA, t \quad (10)$$

SCC results are reported in 2020 U.S. dollars; EUA results are reported in euros for the respective year.

Google Earth Engine implementation and output generation

All remote sensing processing was carried out on the Google Earth Engine cloud-computing platform (Gorelick et al., 2017). The workflow comprised the following sequential steps: (1) delineation of the study area as the intersection of the Manavgat administrative boundary with the MCD64A1-derived event envelope; (2) production of Sentinel-2 pre- and post-fire median composites using dual-layer cloud masking (cloud probability threshold + SCL); (3) computation of dNBR and data-driven severity classification (p33/p67 tertile thresholds); (4) extraction of the forest mask from CLC 2018; (5) reprojection of MOD17A3HGF annual NPP series to EPSG:4326 with the 0.0001 scale factor applied; (6) resampling of 20 m Sentinel-2-derived layers to the MOD17 500 m grid via setDefaultProjection() and reduceResolution(); (7) pixel-level carbon loss computation and DID control-area correction; and (8) generation of economic valuation tables. Principal outputs include: a continuous dNBR map, a severity class map, the analysis mask, the control mask, annual carbon loss rasters, an annual DID net-effect summary, a severity-class area summary, and annual summary tables.

Results

Event envelope and forest mask

The MCD64A1-derived event envelope within the Manavgat administrative boundary covers 424 km^2 and overlaps 270 km^2 of pre-fire forest identified from CLC 2018. Valid paired pre- and post-fire Sentinel-2 observations sufficient for dNBR calculation were retained for 246.26 km^2 of this forest area. The remaining 23.74 km^2 (8.8%) did not retain a valid paired dNBR value after image-quality masking and mask harmonisation and was therefore excluded from severity classification. This residual area represents a no-data/processing subset rather than a fourth burn-severity class. Within the 246.26 km^2 classified area, low-, moderate-, and high-severity classes occupy 62.00, 89.83, and 94.43 km^2, respectively (Table 1).

Fire severity mapping

The Manavgat wildfire, which ignited on 28 July 2021, was spatially characterised using dNBR values derived

Table 1 Study area and severity class area summary

Metric	Value	Unit
Event envelope	424.0	km^2
Pre-fire forest within event envelope	270.0	km^2
Low severity	62.00	km^2
Moderate severity	89.83	km^2
High severity	94.43	km^2
Total classified area	246.26	km^2
Excluded from severity classification (no valid paired dNBR)	23.74	km^2
p33	0.316	dNBR
p67	0.613	dNBR

from Sentinel-2 Surface Reflectance Harmonized imagery (Fig. 1a). In the dNBR map produced from pre-fire (1 June–27 July 2021) and post-fire (1 September–31 October 2021) median composites, pixel values range from −1.238 to +1.362, with a mean of 0.401 (5th percentile: −0.017; 95th percentile: 0.962). Negative dNBR values are concentrated predominantly in river valleys and agricultural areas, while values above 0.70 are clustered on conifer-dominated slopes.

Using the fixed study-area-specific cut-offs p33 = 0.316 and p67 = 0.613, low-severity areas account for 62.00 km^2 (25.2%), moderate-severity areas for 89.83 km^2 (36.5%), and high-severity areas for 94.43 km^2 (38.3%) of the 246.26 km^2 forest area retaining valid paired dNBR observations. Percentages therefore refer to the classified area and exclude the 23.74 km^2 no-data/processing subset (Fig. 1b). This distribution indicates that the fire produced a pronounced severity mosaic across the study area, with moderate- and high-severity burn patterns dominating. Percentages are calculated relative to the 246.26 km^2 classified area.

Reference NPP and pre-fire carbon sink capacity

The 5-year mean of the MOD17A3HGF product for the 2016–2020 reference period yielded an average NPP of 0.830 kg C m^{-2} yr^{-1} across burned cells within the analysis mask, with spatial variability spanning 0.241–1.026 kg C m^{-2} yr^{-1} (Fig. 2). NPP followed a relatively stable trend throughout the

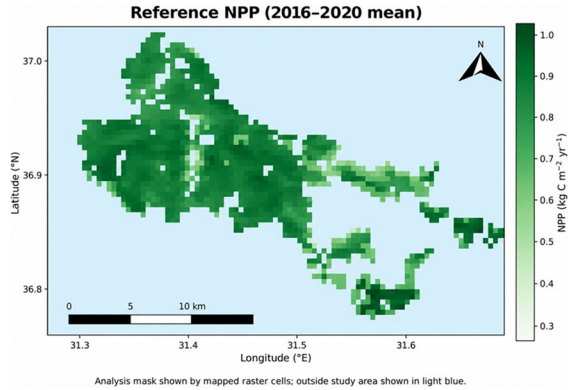

Fig. 2 Mean annual NPP reference map for the 2016–2020 pre-fire period. NPP was derived from MODIS MOD17A3HGF after application of the 0.0001 scale factor. Analysis resolution: 500 m

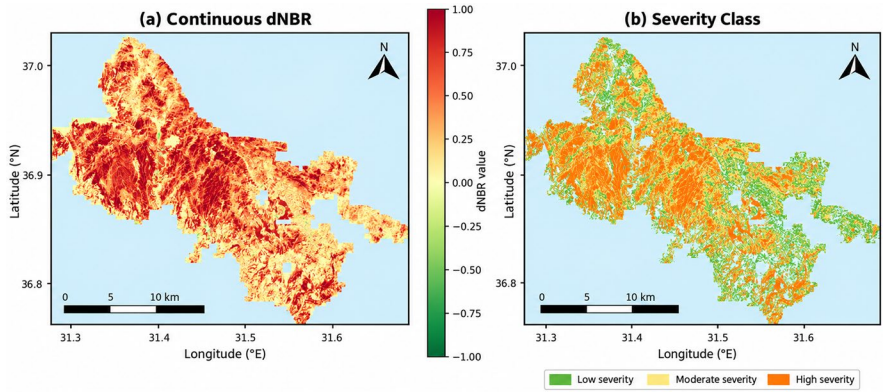

Fig. 1 Spatial patterns of fire effects within the Manavgat wildfire analysis domain. **a** Continuous dNBR derived from pre- and post-fire Sentinel-2 Surface Reflectance Harmonized composites. **b** Relative burn-severity classification based on study-area-specific thresholds derived from the empirical dNBR distribution (p33 = 0.316; p67 = 0.613). Sentinel-2 analysis resolution: 20 m

reference period, peaking at 0.865 kg C m^{-2} in 2018. The value of 0.794 kg C m^{-2} in 2020 likely reflects a relative drought stress episode in the region.

Post-fire NPP change and carbon sink loss

In the fire year 2021, the mean NPP of cells within the analysis mask declined to 0.621 kg C m^{-2} yr^{-1}, corresponding to 74.8% of the reference mean and representing a negative anomaly of 0.209 kg C m^{-2} yr^{-1}. The most pronounced loss, however, was observed in 2022, when post-fire vegetation dieback reached its maximum extent. Mean NPP in 2022 fell to 0.440 kg C m^{-2} yr^{-1}, equivalent to only 53.0% of the reference value and representing a maximum deficit of 0.390 kg C m^{-2} yr^{-1}. In 2023, NPP recovered markedly to 0.705 kg C m^{-2} yr^{-1}, and the recovery rate reached 84.9%. In 2024, NPP was measured at 0.710 kg C m^{-2} yr^{-1}, with the recovery rate remaining at 85.5% (Fig. 3).

Pixel-level carbon loss calculations reveal the spatial distribution of negative ΔNPP values across burned forest cells (Fig. 4). Total carbon losses computed from these calculations are as follows (Table 2): 55,835 t C (204,727 t CO_2e) in 2021; 105,798 t C (387,927 t CO_2e) in 2022; 33,580 t C (123,128 t CO_2e) in 2023; and 31,937 t C (117,103 t CO_2e) in 2024 (Fig. 5). This pattern indicates that the fire impact peaked in the first full post-fire year and that, despite partial recovery in 2023–2024, the carbon sink deficit persisted.

Net effect estimated via difference-in-differences

Net effect values computed using the DID approach confirm that post-fire productivity loss remained substantial even after accounting for the regional climatic background. Annual net effects are: −0.207 kg C m^{-2} in 2021, −0.393 in 2022, −0.124 in 2023, and −0.118 in 2024. The strongest net effect emerged in 2022, with a narrowing but persistent deficit in subsequent years (Table 3). These results strongly corroborate the raw ΔNPP findings in attributing productivity loss to the fire.

Economic valuation of carbon sink loss

The cumulative total carbon loss over the four-year analysis period (2021–2024) is 227,150 t C, equivalent to 832,885 t CO_2e. Under the SC-CO_2 framework, the 4-year cumulative monetary loss amounts

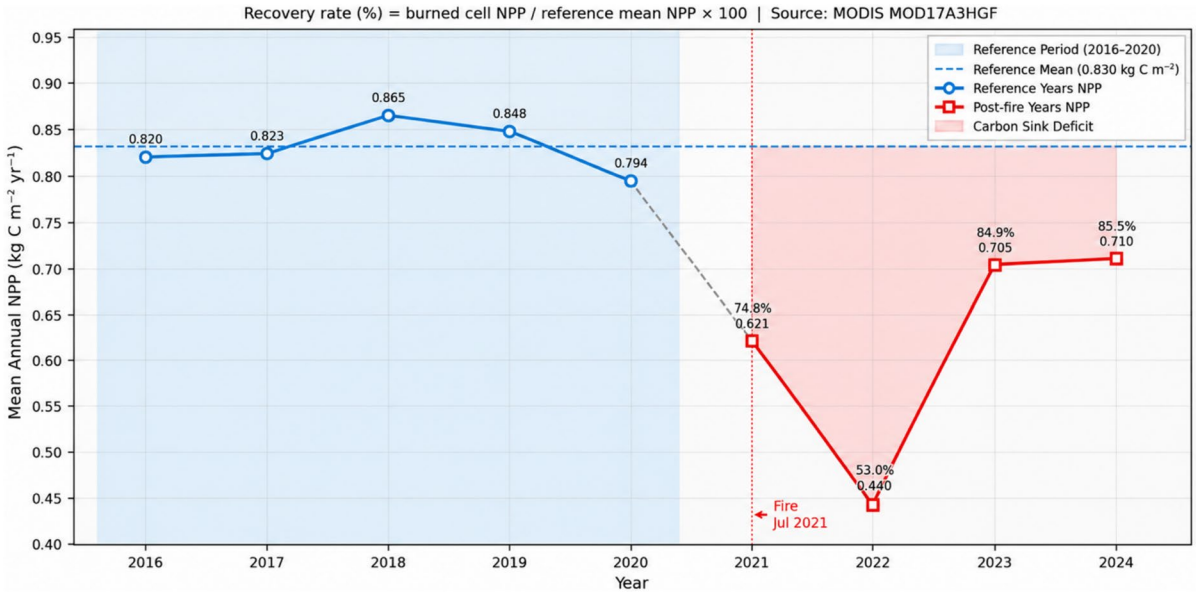

Fig. 3 Annual mean NPP trajectory and post-fire recovery in the analysis cells, 2016–2024. The dashed horizontal line indicates the 2016–2020 reference mean (0.830 kg C m^{-2} yr^{-1}); recovery percentages are shown for the post-fire years

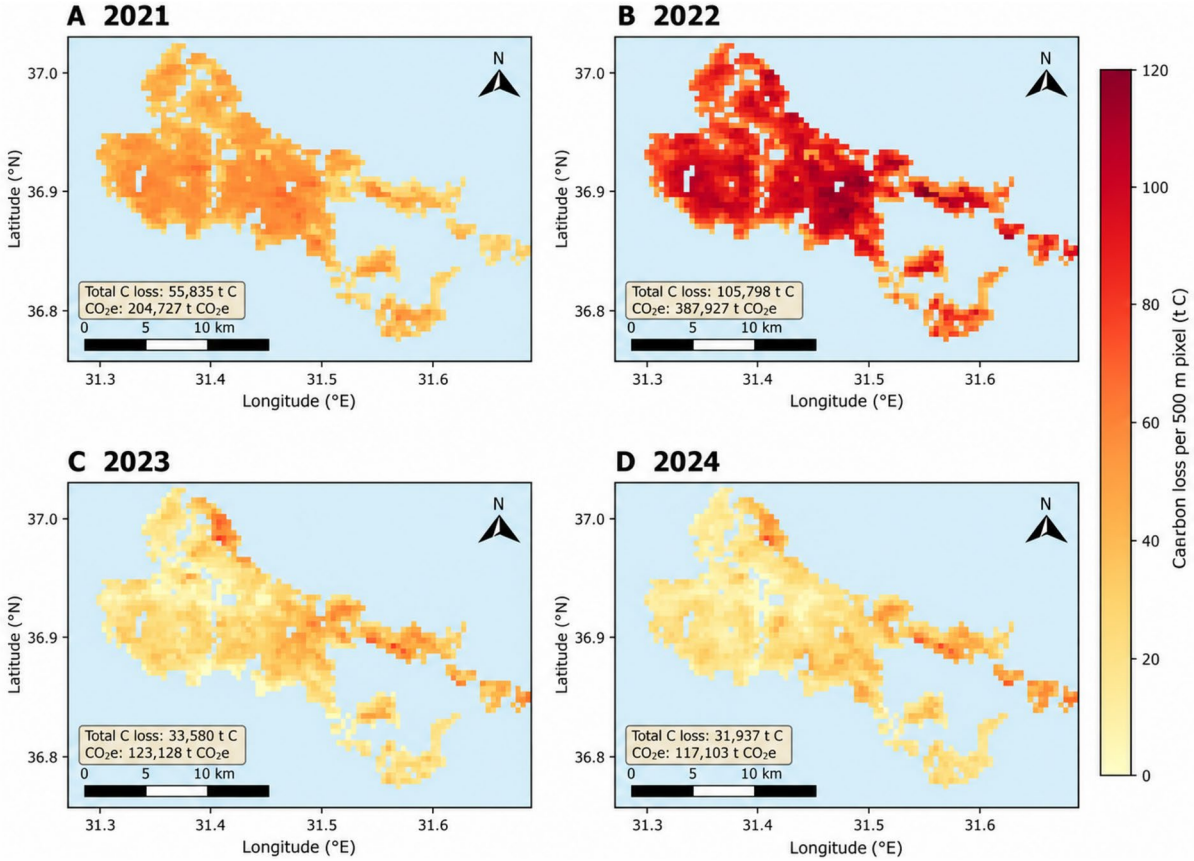

Fig. 4 Annual productivity-based carbon sink loss in the analysis cells, 2021–2024. Panel annotations report the updated annual total carbon loss (t C) and CO_2-equivalent loss (t CO_2e). Analysis resolution: 500 m; source: MODIS MOD17A3HGF

Table 2 Annual carbon loss and recovery summary

Year	Mean NPP (kg C m^{-2} y^{-1})	Recovery (%)	C loss (t C)	CO_2e (t CO_2e)	ΔNPP (kg C m^{-2})
Ref. 2016–2020	0.830	100.0	—	—	0.000
2021	0.621	74.8	55,835	204,727	−0.209
2022	0.440	53.0	105,798	387,927	−0.390
2023	0.705	84.9	33,580	123,128	−0.125
2024	0.710	85.5	31,937	117,103	−0.120

to approximately 99.9 million USD under the low scenario, 158.2 million USD under the central scenario, and 283.2 million USD under the high scenario. Valuation at EUA market prices yields a total economic loss of approximately 60.5 million EUR over the same period (Fig. 6). The peak loss year of 2022 alone implies an economic cost of 73.7 million USD under the central SC-CO_2 value (Table 4).

Discussion

The findings of this study demonstrate that the 2021 Manavgat wildfire not only burned a large area but also produced a pronounced and temporally extended disruption to carbon sink function. The study area covers 424 km^2, of which 270 km^2 was identified as burned forest. Within the classified burned-forest area

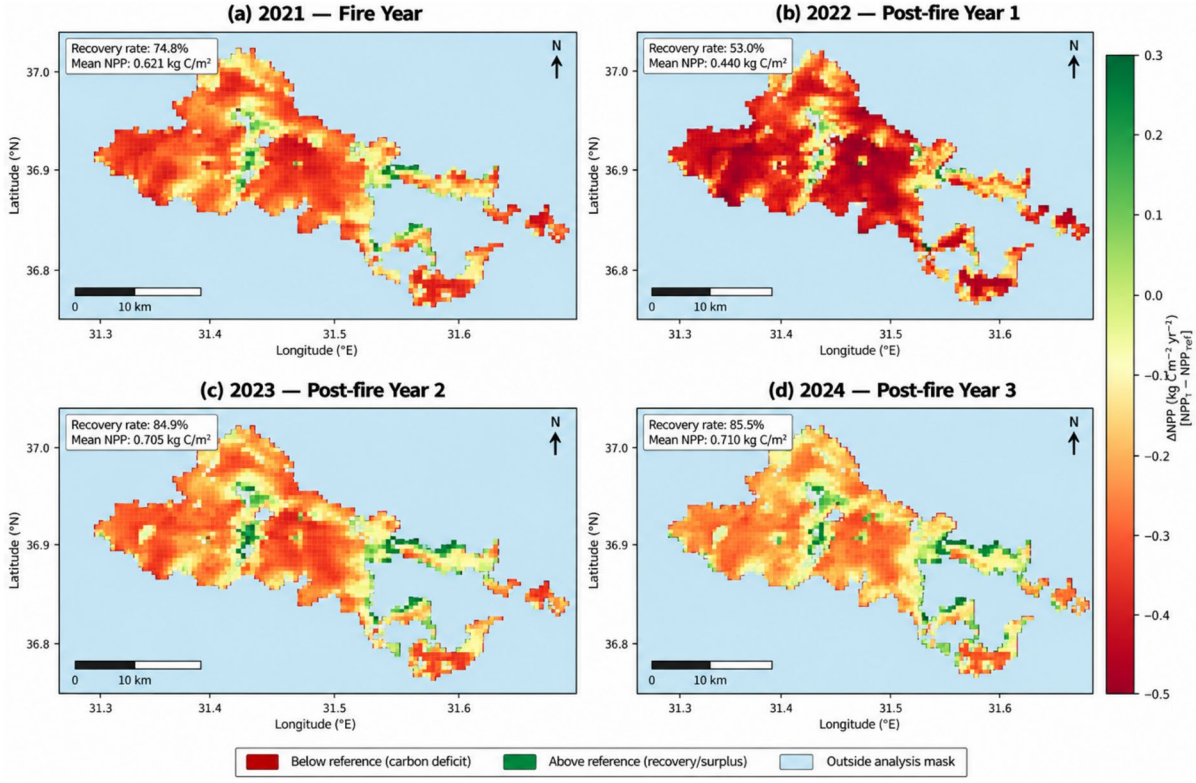

Fig. 5 Annual NPP anomaly (NPP_t − NPP_ref) in the analysis cells, 2021–2024. Negative values indicate productivity deficits relative to the pre-fire reference, whereas positive values indicate recovery above the reference level. Analysis resolution: 500 m

of 246.26 km^2, low-, moderate-, and high-severity classes accounted for 62.00 km^2 (25.2%), 89.83 km^2 (36.5%), and 94.43 km^2 (38.3%), respectively. This distribution indicates that the fire did not generate uniform degradation; rather, moderate- and high-severity burn patterns dominated the severity mosaic. This underscores the inadequacy of treating the burned area solely as a burned/unburned binary and the necessity of interpreting post-fire ecosystem functions within the context of the severity gradient. The effectiveness of dNBR in discriminating such heterogeneous impact patterns has long been established; Miller and Thode (2007) and Chen et al. (2011) in particular showed that spectral difference indices provide a robust analytical basis for interpreting both the spatial distribution of burn impact and subsequent recovery trajectories.

Table 3 Annual net effect estimated via difference-in-differences

Year	DID net effect (kg C m^{-2})
2021	−0.2072
2022	−0.3926
2023	−0.1242
2024	−0.1184

One of the most notable findings of the study is that the largest decline in carbon sink capacity occurred not in the fire year of 2021 but in the following year, 2022. Mean NPP declined to 74.8% of the reference level in 2021, reached its nadir at 53.0% in 2022, and then partially recovered to 84.9% and 85.5% in 2023 and 2024, respectively. This pattern suggests that fire impact extends beyond the immediate combustion loss and that the cumulative effects of canopy mortality, root system damage, water stress, soil moisture deficit, and post-fire climatic stresses can produce "lagged ecological degradation". Drought- and heat-stress-driven productivity suppression in MODIS-derived NPP time series is well documented: Zhao and Running (2010)

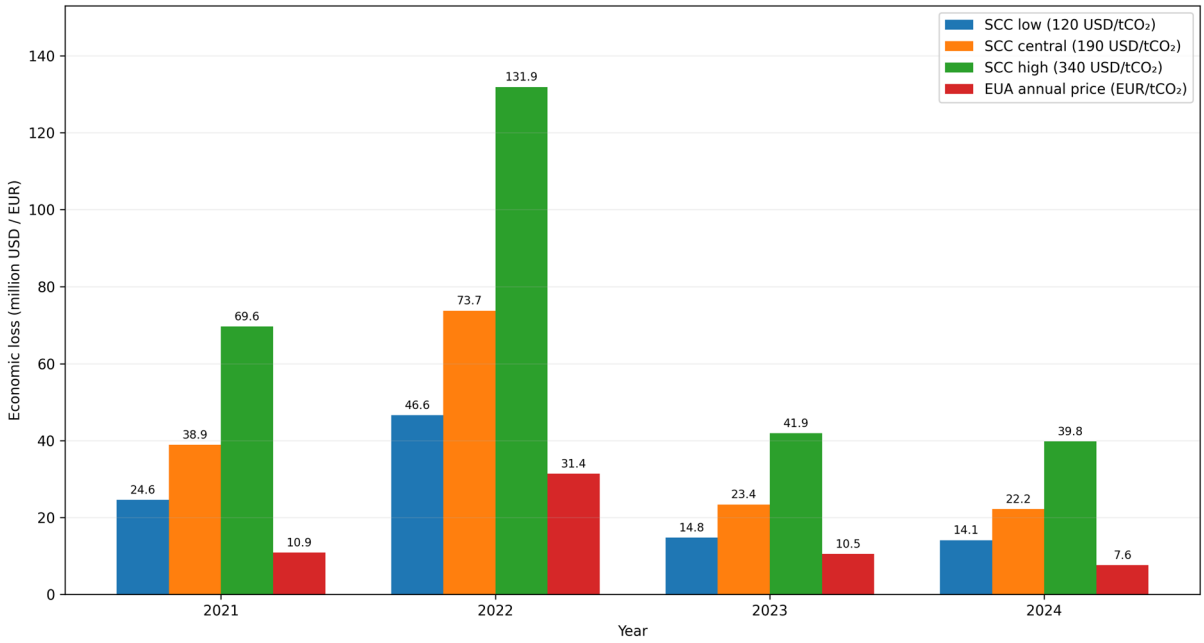

Fig. 6 Scenario-based economic valuation of annual carbon sink loss, 2021–2024. SCC scenarios use 120, 190, and 340 USD tCO_2^{-1}; EUA values use the annual market-price assumptions reported in the Methods

Table 4 Annual and cumulative economic valuation summary

Year	CO_2e (t)	SCC low (M USD)	SCC central (M USD)	SCC high (M USD)	EUA (M EUR)
2021	204,727	24.6	38.9	69.6	10.9
2022	387,927	46.6	73.7	131.9	31.4
2023	123,128	14.8	23.4	41.9	10.5
2024	117,103	14.1	22.2	39.8	7.6
Total	832,885	99.9	158.2	283.2	60.5

demonstrated drought-induced NPP declines at global scale, while Meng et al. (2015) and Fernández-Manso et al. (2016) showed that fire severity and post-fire climate conditions jointly determine recovery rate. More recent work on Mediterranean ecosystems confirms that post-fire recovery in the first few years is highly sensitive to ecosystem type, severity, and recurrent-fire history.

A further important dimension of the findings is that mean NPP had not fully returned to the reference level by 2024. Three years after the fire, productivity-based carbon sink function remained approximately 14.5% below the pre-fire benchmark. This is consistent with the Mediterranean fire ecology literature. Ermitão et al. (2024) and Peña-Molina et al. (2024) show that post-fire recovery in Mediterranean systems is non-linear and that short-term greening frequently does not equate to full restoration of pre-fire functional carbon capacity. The 2023–2024 recovery observed at Manavgat therefore signals the onset of improvement but should not be interpreted as complete restoration of carbon sink capacity. A remote-sensing-based increase in productivity may indicate that the ecosystem is re-establishing itself as a carbon sink, but this does not imply simultaneous recovery of other components—living biomass, deadwood, soil carbon, and net ecosystem carbon balance.

A further methodological contribution of this study is the use of a nearby unburned-forest reference area

to distinguish fire-related productivity change from temporal variability shared across the surrounding landscape. Comparable reference-area designs have previously been applied in satellite-based wildfire studies. Wang and Zhang (2017) used an unburned buffer surrounding the Hayman Fire scar to compare MODIS-derived land-surface phenology inside and outside the burned area, while Wang and Zhang (2020) extended burned-versus-unburned comparisons using MODIS time series across multiple forest fires in the western United States. These studies demonstrate the value of spatially adjacent unburned reference areas for separating disturbance-related vegetation responses from broader temporal variability. The present study builds on this general comparative logic by formalising the burned-versus-reference contrast through a DID estimator applied to annual NPP.

The DID estimates remained very close to the corresponding raw ΔNPP anomalies: −0.207 versus −0.209 kg C m^{-2} in 2021, −0.393 versus −0.390 kg C m^{-2} in 2022, −0.124 versus −0.125 kg C m^{-2} in 2023, and −0.118 versus −0.120 kg C m^{-2} in 2024. This close agreement indicates that the pronounced decline in productivity, particularly the 2022 minimum, cannot be explained solely by temporal variation simultaneously observed in the nearby unburned reference forest. Rather, the control-area adjustment supports the interpretation that the wildfire constituted the dominant disturbance associated with the observed productivity deficit. Nevertheless, this result should not be interpreted as experimental proof of causality. DID inference depends on the comparability of treated and control areas and, particularly, on the parallel-trends assumption (Callaway & Sant'Anna, 2021). Because the present analysis does not constitute a randomised design and does not fully eliminate potential differences between burned and reference forests, the DID estimates are interpreted here as a quasi-experimental robustness check that partially controls for shared temporal variability rather than as complete causal isolation.

The economic valuation findings also constitute a significant contribution of the study. The cumulative 227,150 t C loss, equivalent to 832,885 t CO_2e, corresponds to approximately 99.9, 158.2, and 283.2 million USD under the low, central, and high SCC scenarios, respectively, and approximately 60.5 million EUR under the EUA market-price scenario. These results demonstrate that carbon sink loss is an economic as well as an ecological concern. However, these two economic metrics do not measure the same conceptual quantity: the social cost of carbon represents the expected marginal welfare damage to society from one additional tonne of CO_2 emitted, whereas the EUA price reflects compliance costs and permit scarcity in a regulated carbon market. The economic valuation in this study should accordingly be presented not as a realised monetary loss but as a scenario range produced under two distinct pricing rationales for decision-support purposes.

Viewed in broader perspective, this study contributes to the Mediterranean fire ecology literature in three ways. First, it moves beyond treating fire severity as a spectral damage indicator and links it to carbon sink capacity. Second, it tracks post-fire recovery not from a single-year snapshot but from a multi-year productivity series spanning 2021–2024. Third, it translates the biophysical loss into an economic valuation that can inform decision-making. This triple approach is consistent with recent Mediterranean research on prioritising post-fire restoration actions (Prodromou et al., 2025), indicating that post-fire restoration prioritisation must answer not only "where did the fire burn?" but also "where is function loss greater and more persistent?" From a landscape-planning perspective, such priorities can be situated within broader strategies for climate adaptation, natural-resource protection, and the maintenance of ecosystem services (Duymuş, 2025). This spatially targeted approach is compatible with an integrated ecological-planning perspective that links environmental risk reduction and sustainable disaster resilience (Duymuş et al., 2024).

Conclusions

This study demonstrates that the impact of the 2021 Manavgat wildfire on carbon sink capacity was neither short-lived nor transient. The results show that mean NPP within the burned-forest analysis cells declined markedly in 2021, the largest deficit emerged in 2022, and productivity-based carbon sink function remained below the reference level as late as 2024. The cumulative deficit of 227,150 t C and 832,885 t CO_2e over the 4-year period confirms that the fire produced not merely a fire-year impact but a

persistent pressure on the carbon cycle in subsequent years.

Three management-oriented recommendations emerge from these findings. First, post-fire restoration and monitoring activities should follow a severity-based prioritisation framework. In this fire, where moderate- and high-severity classes dominated the classified burned-forest area, cells exhibiting the highest dNBR values should be treated as priority monitoring units for soil conservation, erosion control, natural regeneration tracking, and active restoration where appropriate. Severity-based prioritisation tools in Mediterranean ecosystems have been shown to improve resource allocation efficiency and to enhance the spatial disaggregation of recovery risk.

Second, post-fire monitoring must be extended over a longer time horizon. The present results show that 3 years of recovery did not fully restore carbon sink capacity. A monitoring design spanning at least 5–10 years, combining NPP/GPP indicators with higher-resolution Sentinel-2/Landsat time series and, where feasible, field-based sampling, is therefore recommended. Such an approach is necessary to distinguish short-term greening from functional carbon recovery. Mediterranean post-fire recovery literature indicates that remote sensing signals alone can sometimes paint an overly optimistic picture of actual ecosystem function.

Third, the carbon sink dimension of post-fire ecosystem loss should be incorporated into forest planning frameworks. Although the SCC- and EUA-based estimates rest on different rationales, both indicate that post-fire sink loss generates substantial societal costs. When post-fire intervention budgets are set, therefore, not only timber production or area rehabilitation but also the lost carbon sink service should be considered, particularly under climate-focused funding mechanisms and nature-based solution investments.

Limitations

Spatial resolution, event-envelope delineation, and scale mismatch

Two spatial-resolution limitations should be distinguished. First, the MCD64A1 product used to define the event-level burn envelope has a spatial resolution of 500 m and may therefore omit small peripheral burned patches or generalise the geometry of the actual fire boundary. Accordingly, the MCD64A1-derived geometry should be interpreted as a broad event envelope rather than as a pixel-accurate representation of the wildfire perimeter. Sentinel-2-derived dNBR at a 20 m analysis scale was used to characterise fine-scale spatial variation in fire severity within this envelope. A burned-area boundary derived directly from Sentinel-2 would provide greater spatial precision and would be preferable for analyses in which exact perimeter geometry and small peripheral patches are primary objectives.

Second, carbon-sink capacity was quantified using the 500 m MOD17A3HGF NPP product, whereas fire severity was characterised at 20 m. Although scale harmonisation and the burned-fraction criterion were used to reduce mixed-pixel effects, these procedures cannot completely eliminate spatial aggregation uncertainty. Consequently, these spatial-resolution constraints may influence absolute area and carbon-loss estimates more strongly than the direction of the observed multi-year productivity response.

NPP as a proxy for carbon sink capacity

In this study, carbon sink capacity is represented by annual NPP rather than net ecosystem exchange or total carbon stock. While NPP is a robust indicator of vegetation productivity and biomass accumulation, it does not fully capture deadfall dynamics, heterotrophic respiration, soil organic carbon, or post-fire decomposition processes. Results reported here should therefore be read as changes in productivity-based carbon sink function rather than as a full carbon budget. This distinction is important to state explicitly, since in some systems short-term greening may be observed even when the total ecosystem carbon balance takes longer to recover.

Study-area-specific thresholds in fire severity classification

The severity classes used in this study were based on fixed, study-area-specific thresholds derived from the empirical dNBR distribution rather than on externally prescribed absolute severity thresholds. The p33 and

p67 values were calculated from the valid burned-forest pixels and then applied consistently throughout the classification domain. This relative classification is useful for distinguishing internal severity gradients within the Manavgat fire; however, because the thresholds depend on the spectral distribution of this particular event, the resulting classes are not directly equivalent to absolute severity classes used in other fires or studies. Moreover, the classification was not calibrated against field-based Composite Burn Index (CBI) measurements. The low-, moderate-, and high-severity labels should therefore be interpreted as relative, study-specific severity categories rather than absolute biophysical severity levels.

DID design assumptions and control area representativeness

While the control area design is a strength of the study, it rests on certain assumptions from a causal-inference perspective. The parallel-trends assumption in particular requires that control and treated areas would have exhibited similar NPP dynamics in the absence of the fire. The results indicate that control-area correction yields a more conservative net effect than raw ΔNPP estimates; however, additional robustness checks such as a pre-trend test, alternative buffer widths, or matched-control sampling may be requested by reviewers. Moreover, unburned forest cells in the 5 km buffer ring may not be entirely independent of fire-related spillover effects from smoke, heat, management interventions, or indirect hydrological effects. DID results therefore provide a robust cross-check but should be presented as a quasi-experimental approach that attempts to separate the fire effect from the climatic background, rather than as full causal isolation.

Scenario-dependent economic valuation

Reporting the economic value of carbon loss via SCC and EUA is a meaningful contribution, but the results are scenario-dependent. SCC values are sensitive to discount rates, damage functions, and long-run climate–economy assumptions, while EUA prices can fluctuate markedly across years depending on regulatory design, market expectations, and permit supply. Because one metric represents societal marginal damage and the other market-based compliance cost, the two indicators should not be interpreted as measuring the same conceptual quantity. The most accurate framing is that the economic valuation provides a scenario range for decision-support reference.

Acknowledgements The author acknowledges the use of openly available Sentinel-2, MODIS (MCD64A1, MOD17A3HGF), and CORINE Land Cover datasets, as well as the Google Earth Engine cloud-computing platform, which made this analysis possible. This study was supported by the project titled "EPD-NET: Filling the Gap: Development of Ecological Planning and Design Learning Network and Adaptive Smart Training Module for Disaster Resilient and Sustainable Cities" (GAP-101183961). The European Commission's support for the production of this publication does not constitute an endorsement of the contents, which reflect the views only of the authors. The Commission cannot be held responsible for any use which may be made of the information contained therein. Additional support was provided by the Eskişehir Technical University Scientific Research Projects Commission under Grant No. 25ADP257.

Author contribution Halil Duymuş confirms that all stages of the study were carried out by the author. The author was responsible for the conceptualization and design of the research, data acquisition, preprocessing of satellite imagery, Google Earth Engine-based analyses, fire severity assessment, carbon sink capacity calculations, interpretation of the results, preparation of figures and tables, writing of the original manuscript, and final revision of the manuscript. The author has read and approved the final version of the manuscript, submitted to Environmental Monitoring and Assessment.

Funding The study received support through the EPD-NET project (GAP-101183961) and the Eskişehir Technical University Scientific Research Projects Commission (Grant No. 25ADP257), as stated in the Acknowledgements.

Data availability The Google Earth Engine scripts, derived raster outputs, and analysis tables generated during the current study are available from the corresponding author upon reasonable request. Sentinel-2, MODIS, and CORINE data used as inputs are openly available from their original providers.

Code availability Google Earth Engine code used in the analyses will be provided upon reasonable request.

Declarations

Conflict of interest The authors declare no competing interests.

Consent to participate and consent for publication Not applicable. The author agrees with the content and consents to submission and publication.

Artificial intelligence statement In this study, artificial intelligence tools were used solely to assist with the language and clarity of the manuscript. They did not play any role in the design, analysis, interpretation, or generation of the scientific results, all of which are the responsibility of the author.

References

Ali, E., Cramer, W., Carnicer, J., Georgopoulou, E., Hilmi, N. J. M., Le Cozannet, G., & Lionello, P. (2022). Cross-chapter paper 4: Mediterranean region. In H.-O. Pörtner, D. C. Roberts, M. Tignor, E. S. Poloczanska, K. Mintenbeck, A. Alegría, M. Craig, S. Langsdorf, S. Löschke, V. Möller, A. Okem, & B. Rama (Eds.), *Climate change 2022: Impacts, adaptation and vulnerability* (pp. 2233–2272). Cambridge University Press. https://doi.org/10.1017/9781009325844.021

Altay, M., & Türker, M. (2026). Assessing burned area and severity in Mediterranean forests using bi-temporal Sentinel-2 and CORINE data: The Manavgat 2021 wildfire case. *Türk Uzaktan Algılama Ve CBS Dergisi, 7*(1), 145–165. https://doi.org/10.48123/rsgis.1775666

Aydın-Kandemir, F., & Demir, N. (2023). 2021 Turkey mega forest fires: Biodiversity measurements of the IUCN Red List wildlife mammals in Sentinel-2 based burned areas. *Advances in Space Research, 71*(7), 3060–3075. https://doi.org/10.1016/j.asr.2023.01.031

Bayer, P., & Aklin, M. (2020). The European Union Emissions Trading System reduced CO_2 emissions despite low prices. *Proceedings of the National Academy of Sciences of the United States of America, 117*(16), 8804–8812. https://doi.org/10.1073/pnas.1918128117

Callaway, B., & Sant'Anna, P. H. C. (2021). Difference-in-differences with multiple time periods. *Journal of Econometrics, 225*(2), 200–230. https://doi.org/10.1016/j.jeconom.2020.12.001

Çamalan, G., Akıl, S., & Pekin, M. A. (2023). Using meteorological early warning system (MEUS) and meteorological indices for assessment of Manavgat forest fires occurred in Turkiye July-August 2021. *European Journal of Forest Engineering, 9*(1), 10–25. https://doi.org/10.33904/ejfe.1288070

Chen, X., Vogelmann, J. E., Rollins, M., Ohlen, D., Key, C. H., Yang, L., Huang, C., & Shi, H. (2011). Detecting post-fire burn severity and vegetation recovery using multitemporal remote sensing spectral indices and field-collected composite burn index data in a ponderosa pine forest. *International Journal of Remote Sensing, 32*(23), 7905–7927. https://doi.org/10.1080/01431161.2010.524678

Duymuş, H. (2025). İklim değişikliğinin peyzaj tasarımına etkisi: Sürdürülebilirlik, dirençlilik ve adaptasyon yaklaşımları. *Resilience, 9*(1), 141–166. https://doi.org/10.32569/resilience.1572354

Duymuş, H., Çabuk, S. N., & Çabuk, A. (2024). Afetlere dirençli ve sürdürülebilir kentler için ekolojik planlama ve tasarım. In M. Tün (Ed.), *Tehlikeler ve afet dirençli kentler I* (pp. 101–141). Özgür Yayınları. https://doi.org/10.58830/ozgur.pub455.c1947

Ermitão, T., Gouveia, C. M., Bastos, A., & Russo, A. C. (2024). Recovery following recurrent fires across Mediterranean ecosystems. *Global Change Biology, 30*(12), Article e70013. https://doi.org/10.1111/gcb.70013

Feranec, J., Hazeu, G., Christensen, S., & Jaffrain, G. (2007). Corine land cover change detection in Europe (case studies of the Netherlands and Slovakia). *Land Use Policy, 24*(1), 234–247. https://doi.org/10.1016/j.landusepol.2006.02.002

Fernández-Manso, A., Quintano, C., & Roberts, D. A. (2016). Burn severity influence on post-fire vegetation cover resilience from Landsat MESMA fraction images time series in Mediterranean forest ecosystems. *Remote Sensing of Environment, 184*, 112–123. https://doi.org/10.1016/j.rse.2016.06.015

Giglio, L., Boschetti, L., Roy, D. P., Humber, M. L., & Justice, C. O. (2018). The Collection 6 MODIS burned area mapping algorithm and product. *Remote Sensing of Environment, 217*, 72–85. https://doi.org/10.1016/j.rse.2018.08.005

Gorelick, N., Hancher, M., Dixon, M., Ilyushchenko, S., Thau, D., & Moore, R. (2017). Google Earth Engine: Planetary-scale geospatial analysis for everyone. *Remote Sensing of Environment, 202*, 18–27. https://doi.org/10.1016/j.rse.2017.06.031

Harris, N. L., Gibbs, D. A., Baccini, A., Birdsey, R. A., de Bruin, S., Farina, M., Fatoyinbo, L., Hansen, M. C., Herold, M., Houghton, R. A., Potapov, P. V., Requena Suarez, D., Roman-Cuesta, R. M., Saatchi, S. S., Slay, C. M., Turubanova, S. A., & Tyukavina, A. (2021). Global maps of twenty-first century forest carbon fluxes. *Nature Climate Change, 11*(3), 234–240. https://doi.org/10.1038/s41558-020-00976-6

Howe, A. A., Parks, S. A., Harvey, B. J., Saberi, S. J., Lutz, J. A., & Yocom, L. L. (2022). Comparing Sentinel-2 and Landsat 8 for burn severity mapping in western North America. *Remote Sensing, 14*(20), Article 5249. https://doi.org/10.3390/rs14205249

Jones, M. W., Abatzoglou, J. T., Veraverbeke, S., Andela, N., Lasslop, G., Forkel, M., Smith, A. J. P., Burton, C., Betts, R. A., van der Werf, G. R., Sitch, S., Canadell, J. G., Santín, C., Kolden, C., Doerr, S. H., & Le Quéré, C. (2022). Global and regional trends and drivers of fire under climate change. *Reviews of Geophysics, 60*(3), Article e2020RG000726. https://doi.org/10.1029/2020RG000726

Kavzoğlu, T., Çölkesen, İ, Tonbul, H., & Öztürk, M. Y. (2021). Uzaktan algılama teknolojileri ile orman yangınlarının zamansal analizi: 2021 yılı Akdeniz ve Ege yangınları [Temporal analysis of forest fires with remote sensing technologies: Mediterranean and Aegean fires in 2021]. *Orman yangınları: Sebepleri, etkileri, izlenmesi, alınacak önlemler ve rehabilitasyon faaliyetleri* (pp. 219–251). Türkiye Bilimler Akademisi. https://doi.org/10.53478/TUBA.2021.048

Key, C. H., & Benson, N. C. (2006). Landscape assessment (LA). In D. C. Lutes, R. E. Keane, J. F. Caratti, C. H. Key, N. C. Benson, S. Sutherland, & L. J. Gangi (Eds.), *FIREMON: Fire effects monitoring and inventory system* (General Technical Report RMRS-GTR-164-CD, pp. LA-1–LA-55). U.S. Department of Agriculture, Forest Service, Rocky Mountain Research Station. https://research.fs.usda.gov/treesearch/24066. Accessed 29 Oct 2026

MedECC. (2020). *Climate and environmental change in the Mediterranean Basin: Current situation and risks for the future. First Mediterranean Assessment Report*. Union for the Mediterranean, Plan Bleu, and UNEP/MAP. https://doi.org/10.5281/zenodo.4768833

Meng, R., Dennison, P. E., Huang, C., Moritz, M. A., & D'Antonio, C. (2015). Effects of fire severity and post-fire climate on short-term vegetation recovery of mixed-conifer

and red fir forests in the Sierra Nevada Mountains of California. *Remote Sensing of Environment, 171*, 311–325. https://doi.org/10.1016/j.rse.2015.10.024

Miller, J. D., & Thode, A. E. (2007). Quantifying burn severity in a heterogeneous landscape with a relative version of the delta Normalized Burn Ratio (dNBR). *Remote Sensing of Environment, 109*(1), 66–80. https://doi.org/10.1016/j.rse.2006.12.006

Özenen-Kavlak, M., Şenyel Kürkçüoğlu, M. A., Duymuş, H., Öztürk, G. B., Çabuk, S. N., Özcan Tatar, C., & Çabuk, A. (2026). Post-fire effects on LST and UHI: A remote sensing and GIS assessment. *Urban Climate, 67*, Article 102878. https://doi.org/10.1016/j.uclim.2026.102878

Pausas, J. G., & Keeley, J. E. (2021). Wildfires and global change. *Frontiers in Ecology and the Environment, 19*(7), 387–395. https://doi.org/10.1002/fee.2359

Pellegrini, A. F. A., Ahlström, A., Hobbie, S. E., Reich, P. B., Nieradzik, L. P., Staver, A. C., Scharenbroch, B. C., Jumpponen, A., Anderegg, W. R. L., Randerson, J. T., & Jackson, R. B. (2018). Fire frequency drives decadal changes in soil carbon and nitrogen and ecosystem productivity. *Nature, 553*(7687), 194–198. https://doi.org/10.1038/nature24668

Peña-Molina, E., Moya, D., Marino, E., Tomé, J. L., Fajardo-Cantos, Á., González-Romero, J., Lucas-Borja, M. E., & de las Heras, J. (2024). Fire vulnerability, resilience, and recovery rates of Mediterranean pine forests using a 33-year time series of satellite imagery. *Remote Sensing, 16*(10), Article 1718. https://doi.org/10.3390/rs16101718

Prodromou, M., Gitas, I., Mettas, C., Tzouvaras, M., Themistocleous, K., Konstantinidis, A., Pamboris, A., & Hadjimitsis, D. (2025). Remote-sensing-based prioritization of post-fire restoration actions in Mediterranean ecosystems: A case study in Cyprus. *Remote Sensing, 17*(7), Article 1269. https://doi.org/10.3390/rs17071269

Rennert, K., Errickson, F., Prest, B. C., Rennels, L., Newell, R. G., Pizer, W., Kingdon, C., Wingenroth, J., Cooke, R., Parthum, B., Smith, D., Cromar, K., Diaz, D., Moore, F. C., Müller, U. K., Plevin, R. J., Raftery, A. E., Ševčíková, H., Sheets, H., … Anthoff, D. (2022). Comprehensive evidence implies a higher social cost of CO2. *Nature, 610*(7933), 687–692. https://doi.org/10.1038/s41586-022-05224-9

Roy, D. P., Boschetti, L., & Trigg, S. N. (2006). Remote sensing of fire severity: Assessing the performance of the normalized burn ratio. *IEEE Geoscience and Remote Sensing Letters, 3*(1), 112–116. https://doi.org/10.1109/LGRS.2005.858485

Running, S. W., Nemani, R. R., Heinsch, F. A., Zhao, M., Reeves, M., & Hashimoto, H. (2004). A continuous satellite-derived measure of global terrestrial primary production. *BioScience, 54*(6), 547–560. https://doi.org/10.1641/0006-3568(2004)054[0547:ACSMOG]2.0.CO;2

Serrano-Ortiz, P., Marañón-Jiménez, S., Reverter, B. R., Sánchez-Cañete, E. P., Castro, J., Zamora, R., & Kowalski, A. S. (2011). Post-fire salvage logging reduces carbon sequestration in Mediterranean coniferous forest. *Forest Ecology and Management, 262*(12), 2287–2296. https://doi.org/10.1016/j.foreco.2011.08.023

U.S. Environmental Protection Agency. (2023). *Report on the social cost of greenhouse gases: Estimates incorporating recent scientific advances.* https://www.epa.gov/system/files/documents/2023-12/epa_scghg_2023_report_final.pdf

Wang, J., & Zhang, X. (2017). Impacts of wildfires on interannual trends in land surface phenology: An investigation of the Hayman Fire. *Environmental Research Letters, 12*(5), Article 054008. https://doi.org/10.1088/1748-9326/aa6ad9

Wang, J., & Zhang, X. (2020). Investigation of wildfire impacts on land surface phenology from MODIS time series in the western US forests. *ISPRS Journal of Photogrammetry and Remote Sensing, 159*, 281–295. https://doi.org/10.1016/j.isprsjprs.2019.11.027

Yılmaz, O. S., Acar, U., Balık Şanlı, F., Gülgen, F., & Ateş, A. M. (2023). Mapping burn severity and monitoring CO content in Türkiye's 2021 wildfires, using Sentinel-2 and Sentinel-5P satellite data on the GEE platform. *Earth Science Informatics, 16*(1), 221–240. https://doi.org/10.1007/s12145-023-00933-9

Zhao, M., Heinsch, F. A., Nemani, R. R., & Running, S. W. (2005). Improvements of the MODIS terrestrial gross and net primary production global data set. *Remote Sensing of Environment, 95*(2), 164–176. https://doi.org/10.1016/j.rse.2004.12.011

Zhao, M., & Running, S. W. (2010). Drought-induced reduction in global terrestrial net primary production from 2000 through 2009. *Science, 329*(5994), 940–943. https://doi.org/10.1126/science.1192666

Zhu, Z., Wang, S., & Woodcock, C. E. (2015). Improvement and expansion of the Fmask algorithm: Cloud, cloud shadow, and snow detection for Landsats 4–7, 8, and Sentinel 2 images. *Remote Sensing of Environment, 159*, 269–277. https://doi.org/10.1016/j.rse.2014.12.014

Publisher's Note Springer Nature remains neutral with regard to jurisdictional claims in published maps and institutional affiliations.

Springer Nature or its licensor (e.g. a society or other partner) holds exclusive rights to this article under a publishing agreement with the author(s) or other rightsholder(s); author self-archiving of the accepted manuscript version of this article is solely governed by the terms of such publishing agreement and applicable law.